Supplementary Information for

Drawing a Clear Mechanistic Picture for the Aggregation-Induced Emission Process

Haoke Zhang,‡[abc] Junkai Liu,‡[abc] Lili Du,[de] Chao Ma,[f] Nelson L. C. Leung,[abc] Yingli Niu,[g] Anjun Qin,[h] Jingzhi Sun,[i] Qian Peng,[g] Herman H. Y. Sung,[a] Ian D. Williams,[a] Ryan T. K. Kwok,[abc] Jacky W. Y. Lam,[abc] Kam Sing Wong,[f] David Lee Phillips,[d] and Ben Zhong Tang*[abch]

[a]Department of Chemistry, The Hong Kong University of Science and Technology (HKUST), Clear Water Bay, Kowloon, Hong Kong, China. E-mail: tangbenz@ust.hk
[b]The Hong Kong Branch of Chinese National Engineering Research Center for Tissue Restoration and Reconstruction, HKUST, Clear Water Bay, Kowloon, Hong Kong, China
[c]HKUST-Shenzhen Research Institute, No. 9 Yuexing 1st RD, South Area, Hi-tech Park Nanshan, Shenzhen 518057, China
[d]Department of Chemistry, The University of Hong Kong, Pokfulam Road, Hong Kong, China
[e]Institute of Life Sciences, Jiangsu University, Zhenjiang 212013, China
[f]Department of Physics, HKUST, Clear Water Bay, Kowloon, Hong Kong, China
[g]Department of Physics, School of Science, Beijing Jiaotong University, Shangyuancun No. 3, Beijing 100044, China
[h]Center for Aggregation-Induced Emission, SCUT-HKUST Joint Research Institute, State Key Laboratory of Luminescent Materials and Devices, South China University of Technology, Guangzhou 510640, China
[i]MOE Key Laboratory of Macromolecular Synthesis and Functionalization, Department of Polymer Science and Engineering, Zhejiang University, Hangzhou 310027, China
[g]Key Laboratory of Organic Solids, Beijing National Laboratory for Molecular Science, Institute of Chemistry, Chinese Academy of Sciences, Beijing 100190, China

*Corresponding author. Email: tangbenz@ust.hk

‡ These two authors contributed equally to this work

This PDF file includes:

Figure S1. Synthetic routes for 2,4,6-TMe-DPE, 2,6-DMe-DPE, 2,4,6-TMe-TPh, 2,4,5-TMe-DPE, 2,5-DMe-DPE and 2,4,5-TMe-TPh.
Figure S2. ^{1}H NMR spectra of 2,5-DMe-DPE in $CDCl_3$. The solvent peaks were marked as asterisk.
Figure S3. ^{13}C NMR spectra of 2,5-DMe-DPE in $CDCl_3$. The solvent peak was marked as asterisk.
Figure S4. ^{1}H NMR spectra of 2,6-DMe-DPE in $CDCl_3$. The solvent peaks were marked as asterisk.
Figure S5. ^{13}C NMR spectra of 2,6-DMe-DPE in $CDCl_3$. The solvent peak was marked as asterisk.
Figure S6. ^{1}H NMR spectra of 2,4,5-TMe-DPE in $CDCl_3$. The solvent peaks were marked as asterisk.
Figure S7. ^{13}C NMR spectra of 2,4,5-TMe-DPE in $CDCl_3$. The solvent peak was marked as asterisk.
Figure S8. ^{1}H NMR spectra of 2,4,6-TMe-DPE in $CDCl_3$. The solvent peaks were marked as asterisk.
Figure S9. ^{13}C NMR spectra of 2,4,6-TMe-DPE in $CDCl_3$. The solvent peak was marked as asterisk.
Figure S10. ^{1}H NMR spectra of 2,4,5- TMe-TPh in $CDCl_3$. The solvent peaks were marked as asterisk.
Figure S11. ^{13}C NMR spectra of 2,4,5-TPh-TM in $CDCl_3$. The solvent peaks were marked as asterisk.
Figure S12. ^{1}H NMR spectra of 2,4,6-TPh-TM in $CDCl_3$. The solvent peaks were marked as asterisk.
Figure S13. ^{13}C NMR spectra of 2,4,6-TPh-TM in $CDCl_3$. The solvent peak was marked as asterisk.
Figure S14. HRMS spectrum of 2,5-DMe-DPE.
Figure S15. HRMS spectrum of 2,6-DMe-DPE.
Figure S16. HRMS spectrum of 2,4,5-TMe-DPE.
Figure S17. HRMS spectrum of 2,4,6-TMe-DPE.
Figure S18. HRMS spectrum of 2,4,5-TMe-TPh.
Figure S19. HRMS spectrum of 2,4,6-TMe-TPh.
Figure S20. ORTEP plot of molecular structure of 2,4,5-TMe-DPE as determined by X-ray diffraction.
Figure S21. ORTEP plot of molecular structure of 2,4,6-TMe-DPE as determined by X-ray diffraction.
Figure S22. ORTEP plot of molecular structure of 2,4,5-TMe-TPh as determined by X-ray diffraction.
Figure S23. ORTEP plot of molecular structure of 2,4,6-TMe-TPh as determined by X-ray diffraction.
Figure S24. Absorption spectra of (A) 2,4,5-TMe-DPE and (B) 2,4,6-TMe-DPE in THF/water mixtures with water fractions (f_w) = 0 and 90%. Concentration=10^{-4} M.
Figure S25. Crystal packing structures of 2,4,5-TMe-DPE.
Figure S26. Crystal packing structures of 2,4,6-TMe-DPE.
Figure S27. Frontier molecular orbitals of the dimer, trimer and tetramer of 2,4,5-TMe-DPE, 2,4,6-TMe-DPE in the ground state calculated by DFT B3LYP/6-31G**, Gaussian 09 program. Isovalue = 0.01 e/Å^3.
Figure S28. Time-resolved fluorescence decay curves of 2,4,6-TMe-DPE and 2,4,5-TMe-DPE in THF solution with a 290 nm laser source excitation. System limited (~30ps) decay curve of laser source was also recorded for reference. These plots have been smoothed with Adjacent-Averaging method.
Figure S29. Plot of calculated reorganization energy versus the normal mode wavenumber of (A and B) 2,4,6-TMe-DPE and (B) 2,4,5-TMe-DPE in the crystal state calculated by the TD-DFT, B3LYP/6-311G** and Gaussian 09 program. Inset: contribution of bond length, bond angle and dihedral angle to the total reorganization energy.
Figure S30. Absorption spectra of (A) 2,5-DMe-DPE and (B) 2,6-DMe-DPE in THF. Concentration =10^{-5} M.
Figure S31. PL spectra of (A) 2,6-DMe-DPE and (B) 2,5-DMe-DPE in THF/water mixtures with different water fractions (f_w). (C) Plots of relative PL intensity (I/I_0) of 2,6-DMe-DPE and 2,5-DMe-DPE versus the composition of their THF/water mixture. Concentration = 10 μM, λ_{ex} = 280 nm, I_0 = PL intensity at f_w = 0%.
Figure S32. Absorption spectra of (A) 2,4,5-TMe-TPh and (B) 2,4,6-TMe-TPh in THF. Concentration =10^{-5} M.
Figure S33. Absorption spectra of (A) TPE and (B) TPB in THF. Concentration =10^{-5} M.

General information

Tetrahydrofuran (THF) was distilled from sodium benzophenone ketyl under nitrogen immediately prior to use. 5-Bromo-1,2,4-trimethylbenzene, 2-bromomesitylene, 2,5-dimethylbenzaldehyde and benzene-1,4-diboronic acid were obtained from Sigma-Aldrich, tetraphenylethylene and 1,2,4,5-tetraphenylbenzene were free provided by AIEgen Biotech Co., Ltd. 2,6-Dimethylbenzaldehyde and 2,4,6-trimethylbenzaldehyde were purchased form J&K Scientific Ltd.

^{1}H and ^{13}C NMR spectra were measured on a Bruker AVIII 400 MHz NMR spectrometer using deuterated chloroform as solvent and tetramethylsilane (TMS; δ = 0) as an internal reference. High-resolution mass spectra (HRMS) were recorded on a GCT premier CAB048 mass spectrometer system operating in a MALDI-TOF mode. UV spectra were measured on a Varian CARY 50 UV-visible spectrophotometer. Photoluminescence spectra were recorded on a Horiba Fluorolog®-3 spectrofluorometer. Single-crystal X-ray diffraction measurements were conducted on a Bruker-Nonius Smart Apex CCD diffractometer with graphite-monochromated Mo Kα radiation. Absolute fluorescence quantum yield was measured on a Hamamatsu Quantaurus-QY C11347.

Femtosecond Transient Absorption Spectroscopy (fs-TA)

The fs-TA measurements were performed based on a femtosecond Ti:Sapphire regenerative amplified laser system (Spectra Physics, Spitfire-Pro) and an automated data acquisition system (Ultrafast Systems, Helios model). The amplifier was seeded with the 120 fs output from the oscillator (Spectra Physics, Maitai). The probe pulse was obtained by using approximately 5% of the amplified 800 nm output from the Spitfire to generate a white-light continuum (325-650 nm) in a CaF_2 crystal and then this probe beam was split into two parts before traversing the sample. One probe laser beam goes through the sample while the other probe laser beam goes to the reference spectrometer in order to monitor the fluctuations in the probe beam intensity. For the present experiments, the compounds 2,4,5-TMe-DPE and 2,4,6-TMe-DPE in THF solution were excited by a 267 nm pump beam (the third harmonic of the fundamental 800 nm from the regenerative amplifier). Samples of 1 mL solutions were studied in 2 mm path-length cuvette with an absorbance of 0.5 at 267 nm throughout the data acquisition.

Quantum mechanics and molecular mechanics (QM/MM) calculation

All the calculations were performed in Gaussian 09 program, Density functional theory (DFT-B3LYP) was used. When the reorganization energy calculation was carried out to the aggregated state, a combined quantum mechanics and molecular mechanics (QM/MM) approach using Gaussian 09 package. A cluster containing 73 molecules cut from the single crystal structure set up the two-layer oniom model. The central molecule acted as the high layer (QM) at the (TD)B3LYP/6-311G** level, and the surrounding ones were treated as the low layer (MM) using Universal Force Field (UFF). First, the low layer was fixed and only the central molecule was optimized by the (TD)B3LYP/6-311G**.

Synthesis

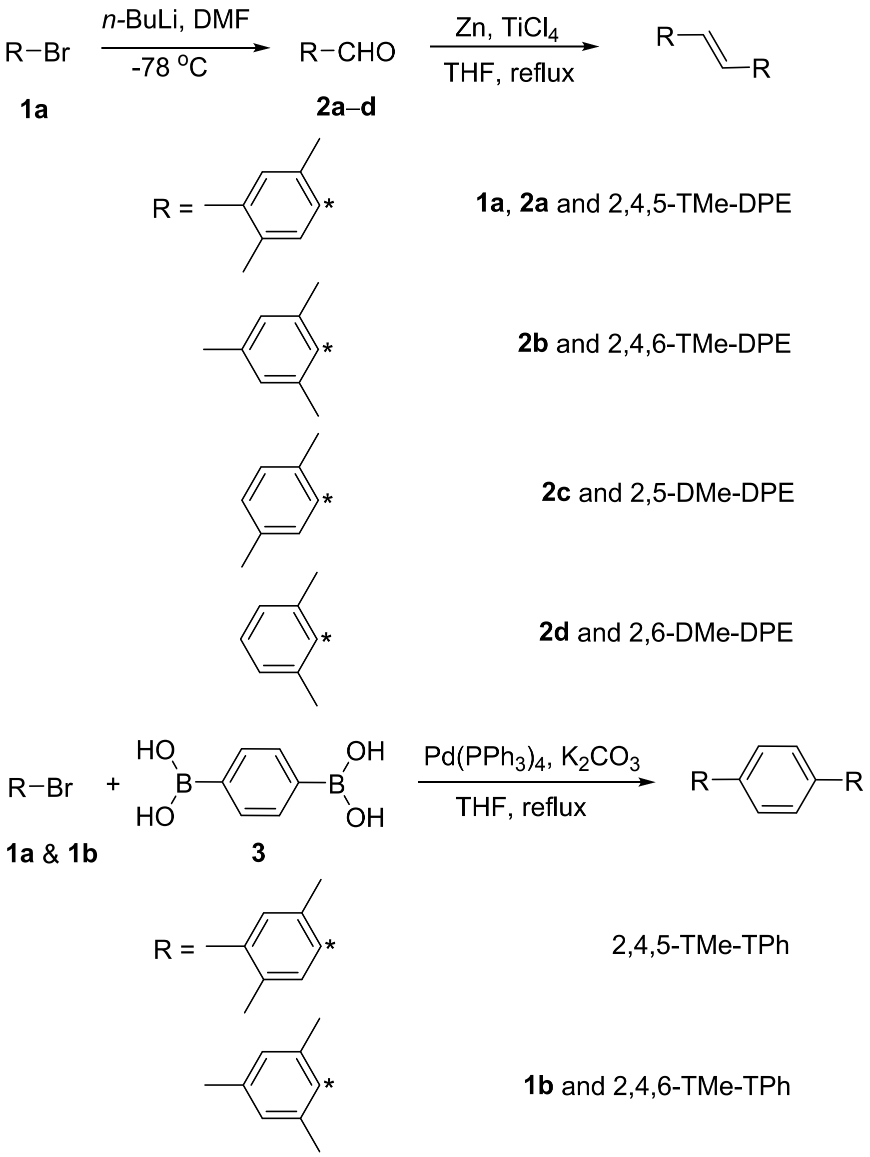

Figure S1. Synthetic routes for 2,4,6-TMe-DPE, 2,6-DMe-DPE, 2,4,6-TMe-TPh, 2,4,5-TMe-DPE, 2,5-DMe-DPE and 2,4,5-TMe-TPh.

2,4,5-Trimethylbenzaldehyde (2a)

1a (10.00 g, 50.23 mmol) was added into a two-necked flask. After degas and refill with nitrogen for three times, 120 mL of distilled THF was injected. The flask was cooled to -78 °C and *n*-butyllithium (25.00 mL, 2.40 M in hexane) was dropwise added into the system. After stirring at -78 °C for 2 h, 7.80 mL of dimethyl formamide was dropwise injected. The mixture was allowed for reaction for another 6 h at -78 °C and was then warmed to room temperature. Saturated NH_4Cl aqueous solution was added to quench the reaction. The mixture was extracted with dichloromethane (DCM). The organic layer was separated, washed with deionized water and brine, and dried over anhydrous sodium sulfate. After filtration, the filtrate was evaporated under reduced pressure and the crude product was purified on a silica gel column using hexane/DCM (5/1, v/v) as eluent. 6.30 g of **2a** was obtained as white powder in 85.0% yield. ^{1}H NMR (400 MHz, $CDCl_3$), δ (TMS, ppm): 10.10 (s, 1H), 7.46 (s, 1H), 6.94 (s, 1H), 2.53 (s, 3H), 2.22 (s, 6H).

(E)-1,2-Bis(2,4,5-trimethylphenyl)ethene (2,4,5-TMe-DPE)

2a (2.00 g, 13.50 mmol) and zinc dust (2.65 g, 40.50 mmol) were added into a two-necked flask with a reflux condenser. After degas and refill with nitrogen for three times. 100 mL of THF was added into the flask. The mixture was cooled to −78 °C and $TiCl_4$ (2.23 mL, 20.25 mmol) was added dropwise by a syringe. The mixture was slowly warmed to room temperature. After stirring for 1 h, the mixture was refluxed for another 24 h. The reaction was quenched with 4% aqueous HCl solution and filtered. The mixture was extracted with DCM. The organic layer was separated, washed with deionized water and brine, and dried over anhydrous sodium sulfate. After filtration, the filtrate was evaporated under reduced pressure and the crude product was purified on a silica gel column using hexane/DCM (5/1, v/v) as eluent. 1.43 g of 2,4,5-TMe-DPE was obtained as white powder in 80.3% yield. ^{1}H NMR (400 MHz, $CDCl_3$), δ (TMS, ppm): 7.38 (s, 2H), 7.14 (s, 2H), 6.98 (s, 2H), 2.39 (s, 6H), 2.30 (s, 6H), 2.27 (s, 6H). ^{13}C NMR (100 MHz, $CDCl_3$), δ (TMS, ppm): 135.82, 134.42, 134.13, 133.08, 131.78, 126.87, 126.62, 19.41, 19.36. HRMS (MALDI-TOF): *m*/*z*: calcd for $C_{20}H_{24}$: 264.1878 [M^+]; found: 264.1872.

(E)-1,2-Dimesitylethene (2,4,6-TMe-DPE)

The synthetic procedure was same with 2,4,5-TMe-DPE. ^{1}H NMR (400 MHz, $CDCl_3$), δ (TMS, ppm): 6.94 (s, 4H), 6.56 (s, 2H), 2.40 (s, 12H), 2.31 (s, 6H). ^{13}C NMR (100 MHz, $CDCl_3$), δ (TMS, ppm): 136.23, 136.02, 134.76, 131.99, 128.72, 21.37, 20.97. HRMS (MALDI-TOF): *m*/*z*: calcd for $C_{20}H_{24}$: 264.1878 [M^+]; found: 264.1879.

(E)-1,2-Bis(2,5-dimethylphenyl)ethene (2,5-DMe-DPE)

The synthetic procedure was same with 2,4,5-TMe-DPE. ^{1}H NMR (400 MHz, $CDCl_3$), δ (TMS, ppm): 7.44-7.38 (m, 2H), 7.18 (s, 2H), 7.09 (d, *J* = 7.7 Hz, 2H), 7.03-7.02 (dd, *J* = 7.8 Hz, 1.8 Hz 2H), 2.40 (s, 6H), 2.37 (s, 6H). ^{13}C NMR (100 MHz, $CDCl_3$), δ (TMS, ppm): 136.64, 135.56, 132.84, 130.33, 128.30, 127.86, 126.14, 21.13, 19.55. HRMS (MALDI-TOF): *m*/*z*: calcd for $C_{18}H_{20}$: 236.1565 [M^+]; found: 236.1567.

(E)-1,2-Bis(2,6-dimethylphenyl)ethene (2,6-DMe-DPE)

The synthetic procedure was same with 2,4,5-TMe-DPE. ^{1}H NMR (400 MHz, $CDCl_3$), δ (TMS, ppm): 7.12 (s, 6H), 6.61 (s, 2H), 2.44 (s, 12H). ^{13}C NMR (100 MHz, $CDCl_3$), δ (TMS, ppm): 136.11, 132.33, 127.94, 126.71, 21.48. HRMS (MALDI-TOF): *m*/*z*: calcd for $C_{18}H_{20}$: 236.1565 [M^+]; found: 236.1568.

1,4-Bis(2,4,5-trimethylphenyl)benzene

1a (2.64 g, 13.26 mmol), **3** (1.00 g, 6.03 mmol) and a catalytic amount of tetrakis(triphenylphosphine) palladium (0.10 g, 0.08 mmol) were added into a two-necked flask fitted with an allihn condenser. The system was degassed and refilled with nitrogen for three times. Then, 60 mL distilled THF was injected, followed with aqueous potassium carbonate solution (0.15 g, 20 mL). After stirring at 85 °C for 24 h., the mixture was extracted with DCM. The organic layer was washed with deionized water and brine, and dried over anhydrous sodium sulfate. After filtration, the filtrate was evaporated under reduced pressure, and the crude product was purified through a silica gel column chromatograph using hexane/DCM (5/1, v/v) as eluent. A white powder was obtained in 75.3% yield (1.42 g, 4.52 mmol). ^{1}H NMR (400 MHz, $CDCl_3$), δ (TMS, ppm): 7.40 (s, 4H), 7.14 (d, J = 8.1 Hz, 4H), 2.35 (*d*, J = 1.4 Hz, 18H). ^{13}C NMR (100 MHz, $CDCl_3$), δ (TMS, ppm): 140.19, 139.25, 135.49, 133.87, 132.60, 131.83, 131.28, 128.94, 19.99, 19.39, 19.26. HRMS (MALDI-TOF): *m*/*z*: calcd for $C_{24}H_{26}$: 314.2035 [M$^+$]; found: 314.2012.

1,4-Bis(2,4,6-trimethylphenyl)benzene

The synthetic procedure was same with 2,4,5-TMe-TPh. ^{1}H NMR (400 MHz, $CDCl_3$), δ (TMS, ppm): 7.18 (s, 4H), 6.99 (s, 4H), 2.36 (s, 6H), 2.08 (s, 12H). ^{13}C NMR (100 MHz, $CDCl_3$), δ (TMS, ppm): 138.55, 138.43, 135.87, 135.48, 128.60, 127.39, 20.43, 20.09. HRMS (MALDI-TOF): *m*/*z*: calcd for $C_{24}H_{26}$: 314.2035 [M$^+$]; found: 314.2039.

Characterization

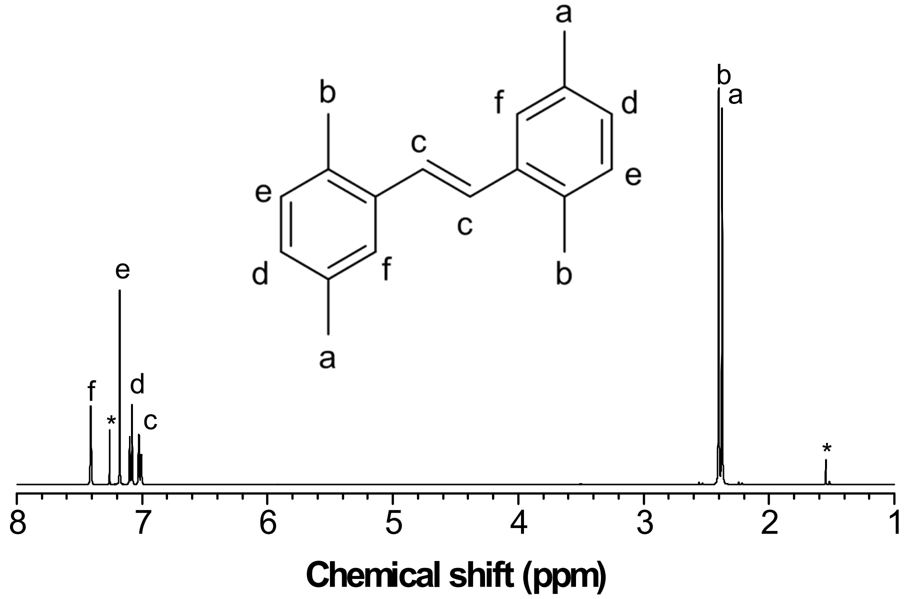

Figure S2. ^{1}H NMR spectra of 2,5-DMe-DPE in $CDCl_3$. The solvent peaks were marked as asterisk.

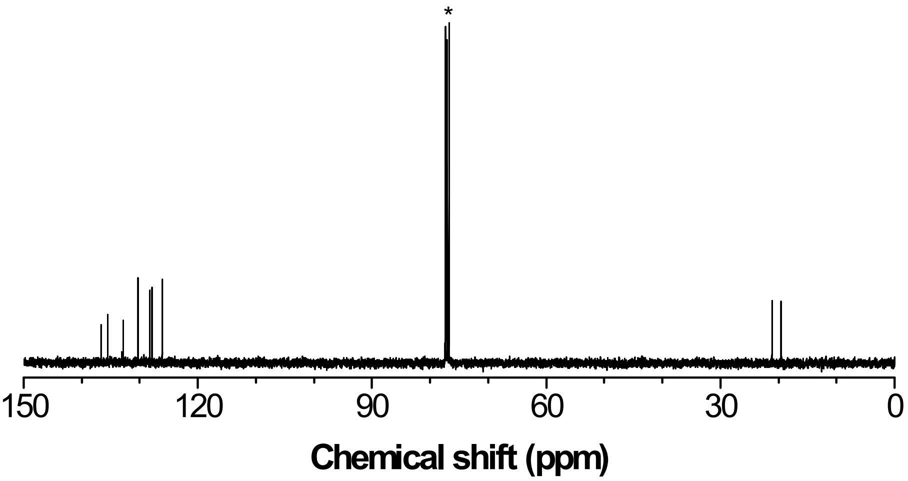

Figure S3. ^{13}C NMR spectra of 2,5-DMe-DPE in $CDCl_3$. The solvent peak was marked as asterisk.

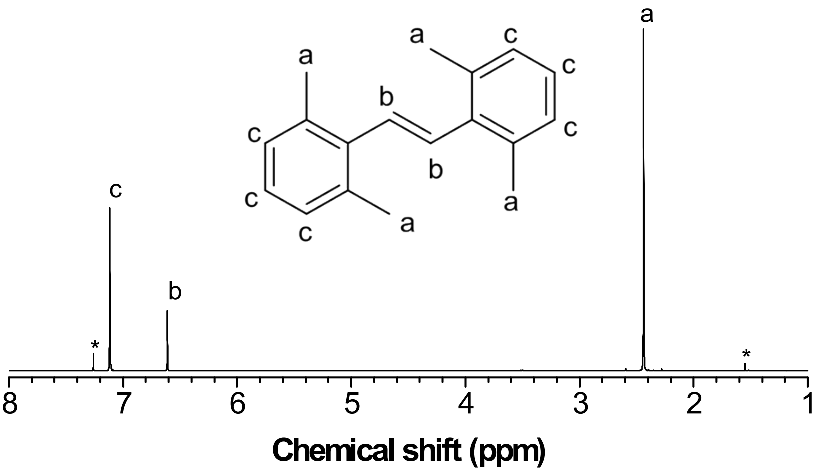

Figure S4. ^{1}H NMR spectra of 2,6-DMe-DPE in $CDCl_3$. The solvent peaks were marked as asterisk.

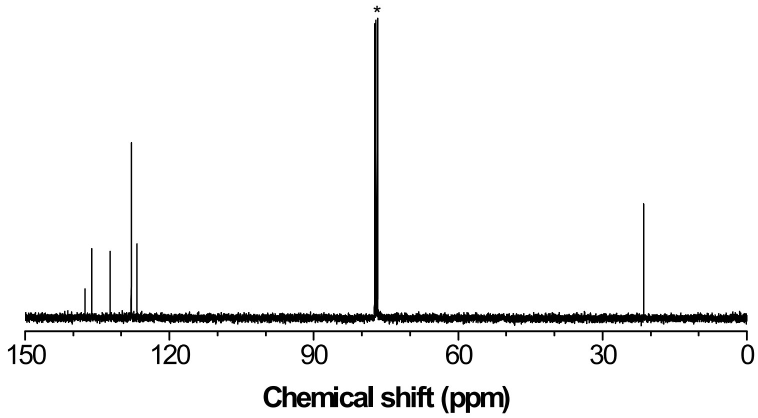

Figure S5. ^{13}C NMR spectra of 2,6-DMe-DPE in $CDCl_3$. The solvent peak was marked as asterisk.

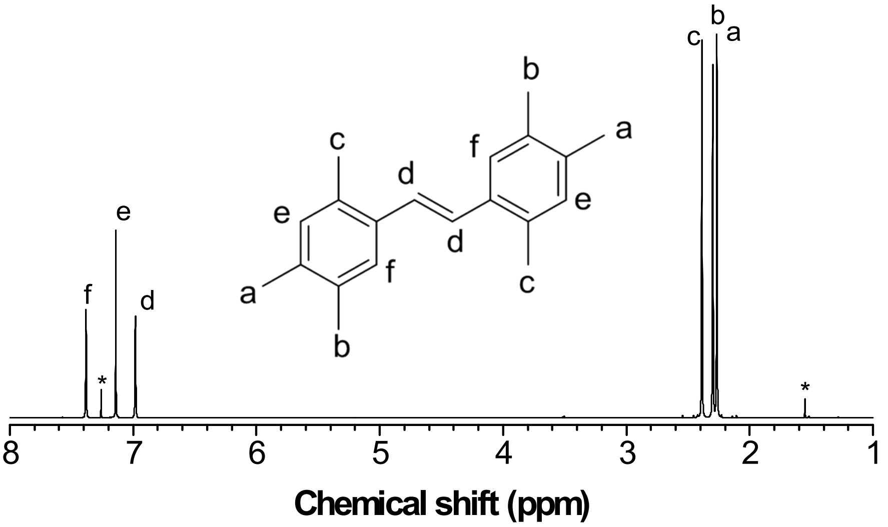

Figure S6. ^{1}H NMR spectra of 2,4,5-TMe-DPE in $CDCl_3$. The solvent peaks were marked as asterisk.

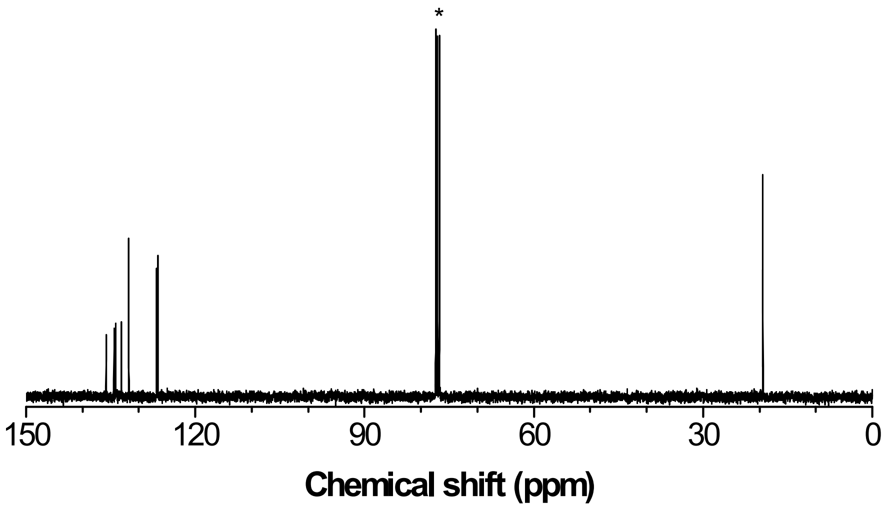

Figure S7. ^{13}C NMR spectra of 2,4,5-TMe-DPE in $CDCl_3$. The solvent peak was marked as asterisk.

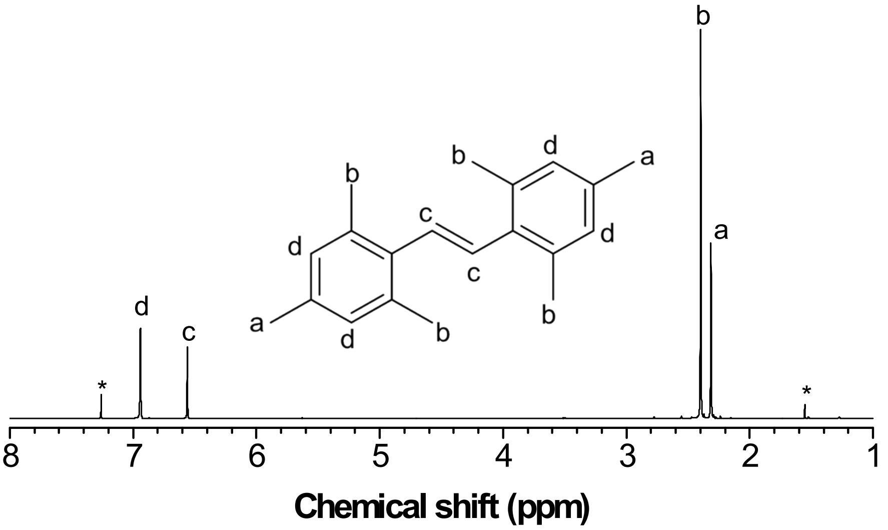

Figure S8. ^{1}H NMR spectra of 2,4,6-TMe-DPE in $CDCl_3$. The solvent peaks were marked as asterisk.

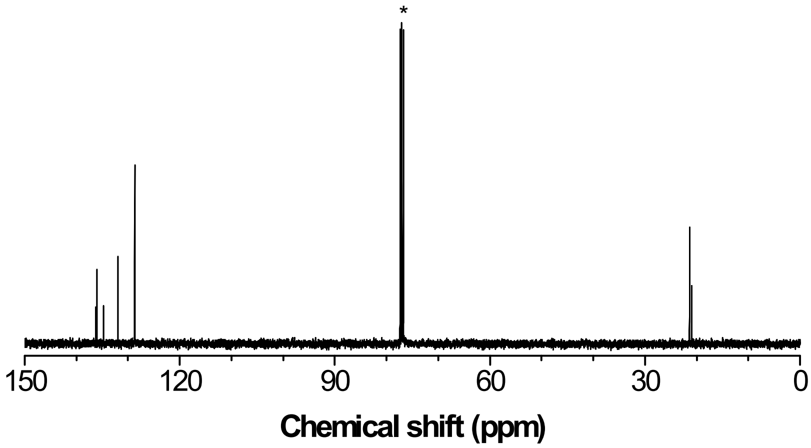

Figure S9. ^{13}C NMR spectra of 2,4,6-TMe-DPE in $CDCl_3$. The solvent peak was marked as asterisk.

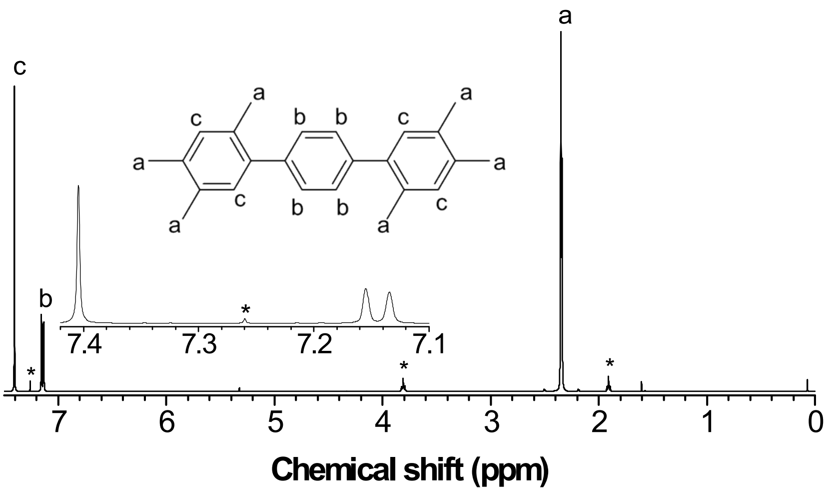

Figure S10. ^1H NMR spectra of 2,4,5- TMe-TPh in $CDCl_3$. The solvent peaks were marked as asterisk.

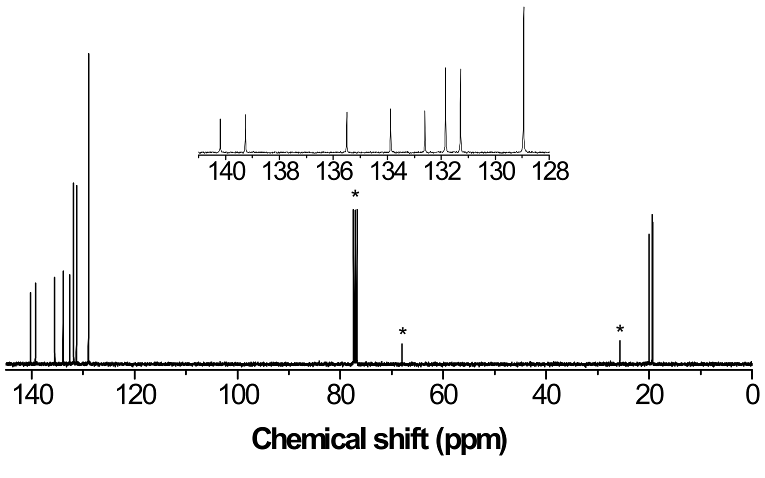

Figure S11. ^{13}C NMR spectra of 2,4,5-TPh-TM in $CDCl_3$. The solvent peaks were marked as asterisk.

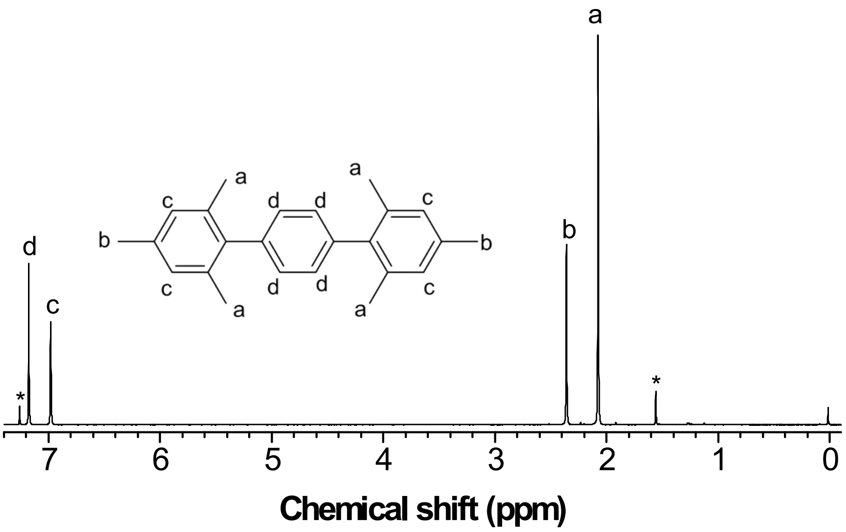

Figure S12. ^{1}H NMR spectra of 2,4,6-TPh-TM in $CDCl_3$. The solvent peaks were marked as asterisk.

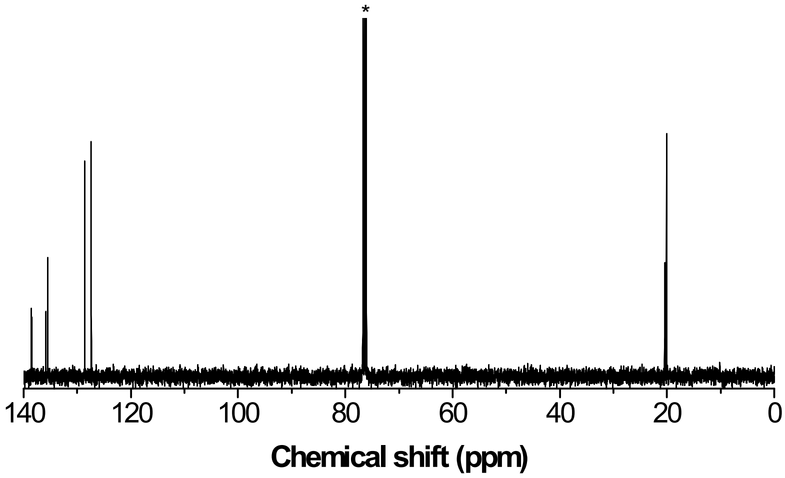

Figure S13. ^{13}C NMR spectra of 2,4,6-TPh-TM in $CDCl_3$. The solvent peak was marked as asterisk.

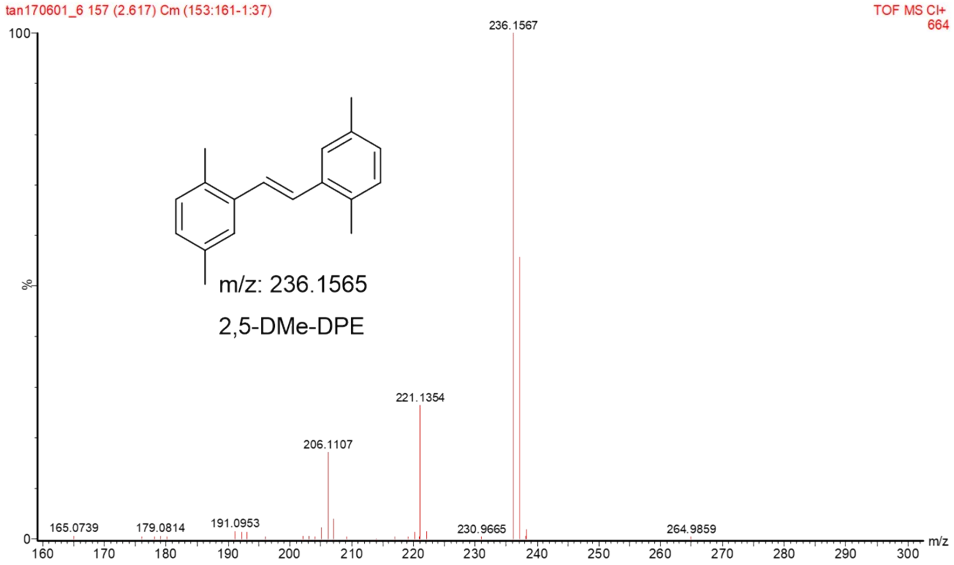

Figure S14. HRMS spectrum of 2,5-DMe-DPE.

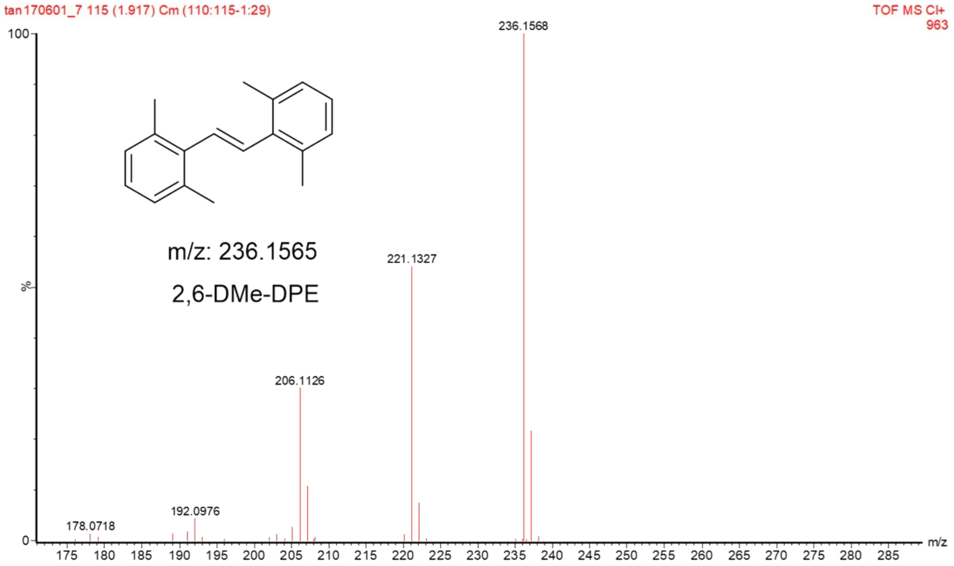

Figure S15. HRMS spectrum of 2,6-DMe-DPE.

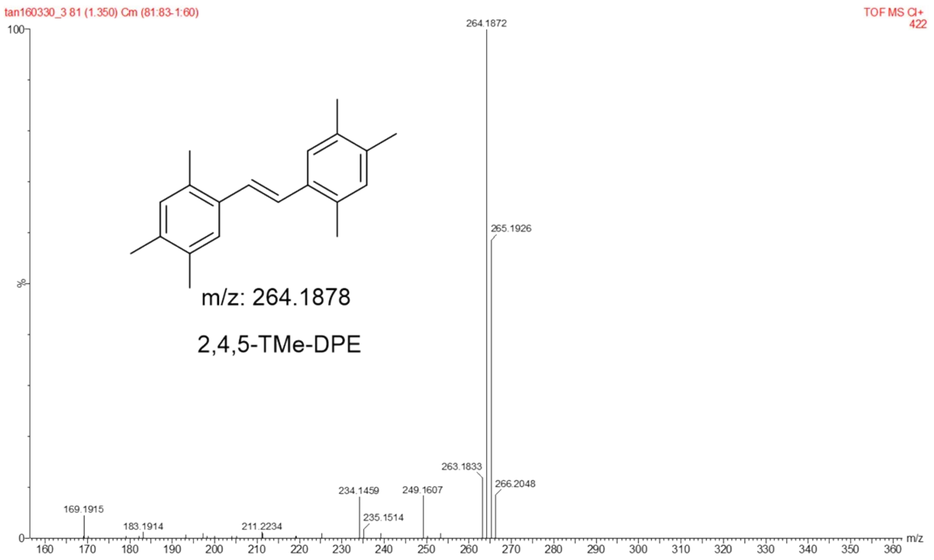

Figure S16. HRMS spectrum of 2,4,5-TMe-DPE.

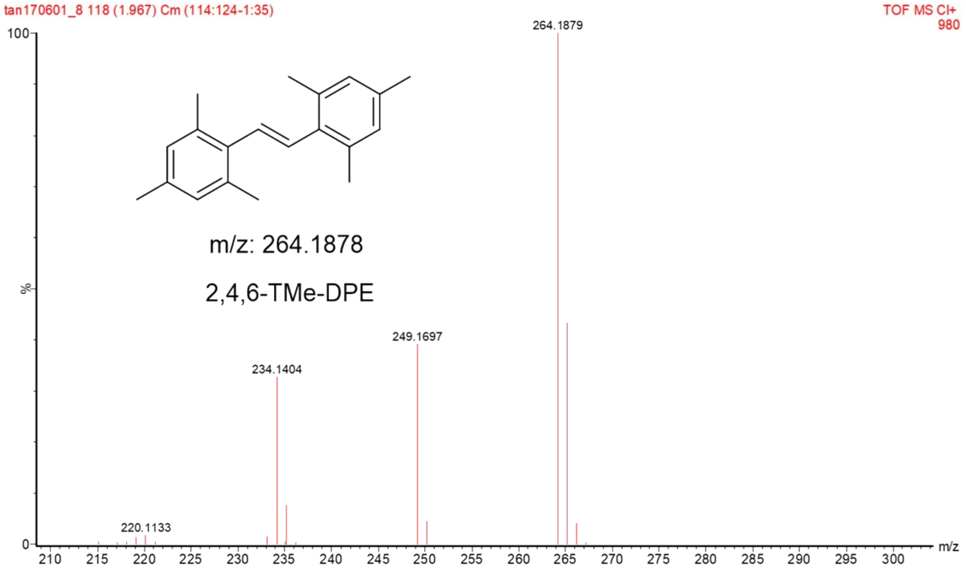

Figure S17. HRMS spectrum of 2,4,6-TMe-DPE.

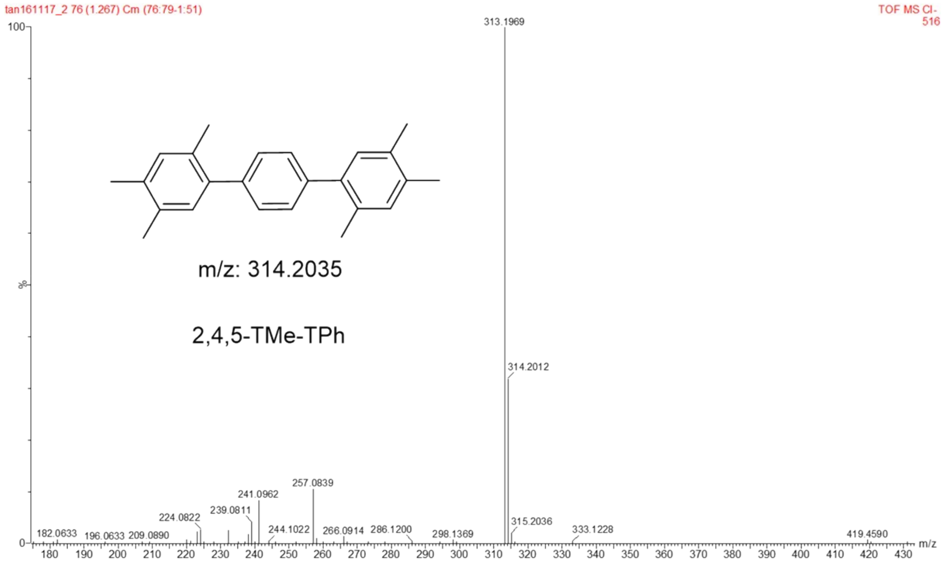

Figure S18. HRMS spectrum of 2,4,5-TMe-TPh.

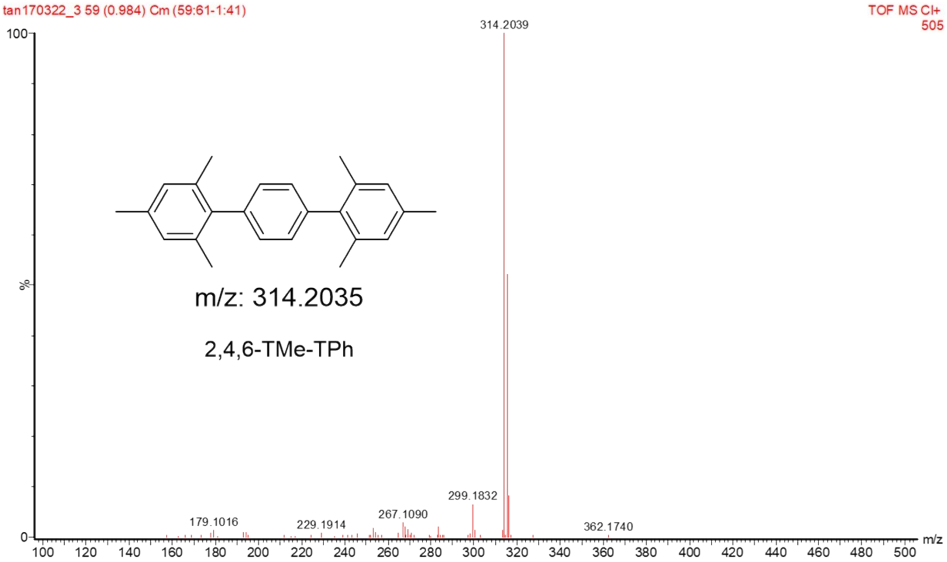

Figure S19. HRMS spectrum of 2,4,6-TMe-TPh.

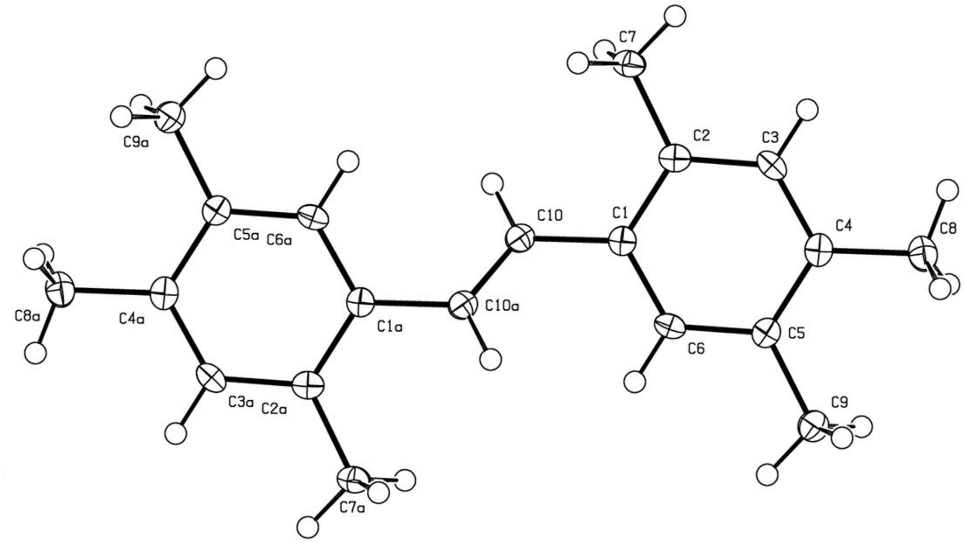

Figure S20. ORTEP plot of molecular structure of 2,4,5-TMe-DPE as determined by X-ray diffraction.

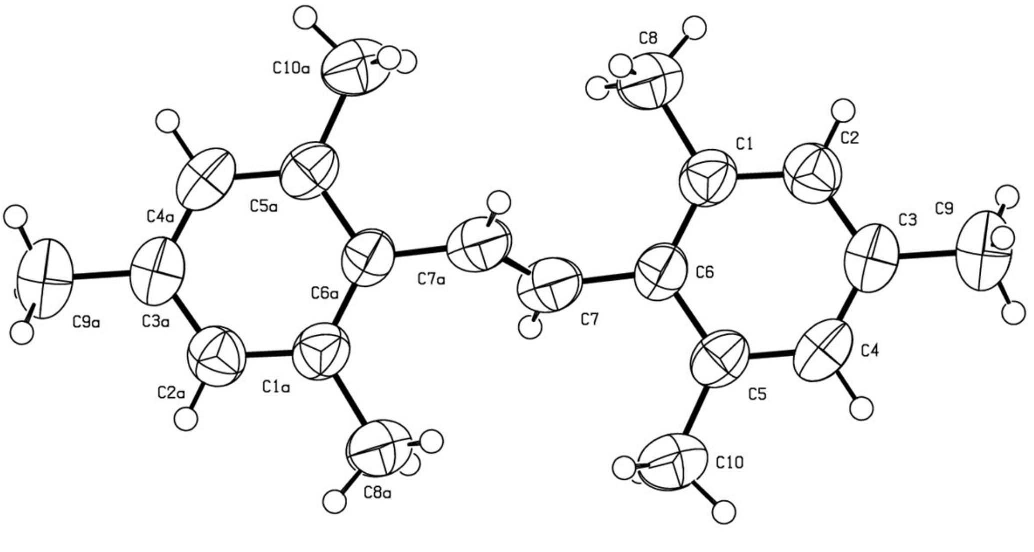

Figure S21. ORTEP plot of molecular structure of 2,4,6-TMe-DPE as determined by X-ray diffraction.

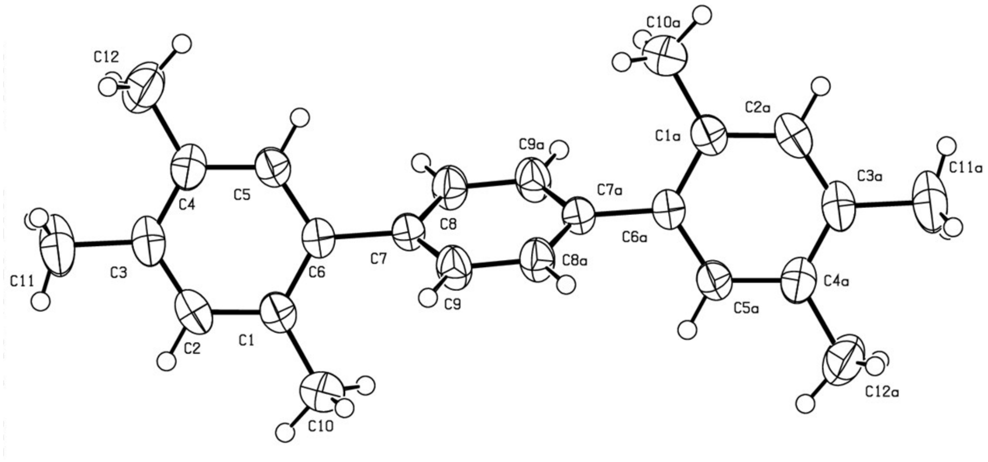

Figure S22. ORTEP plot of molecular structure of 2,4,5-TMe-TPh as determined by X-ray diffraction.

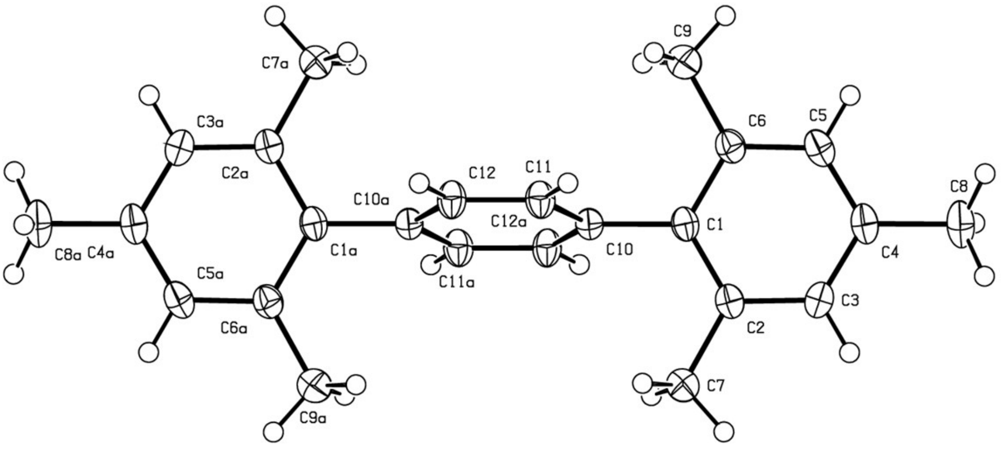

Figure S23. ORTEP plot of molecular structure of 2,4,6-TMe-TPh as determined by X-ray diffraction.

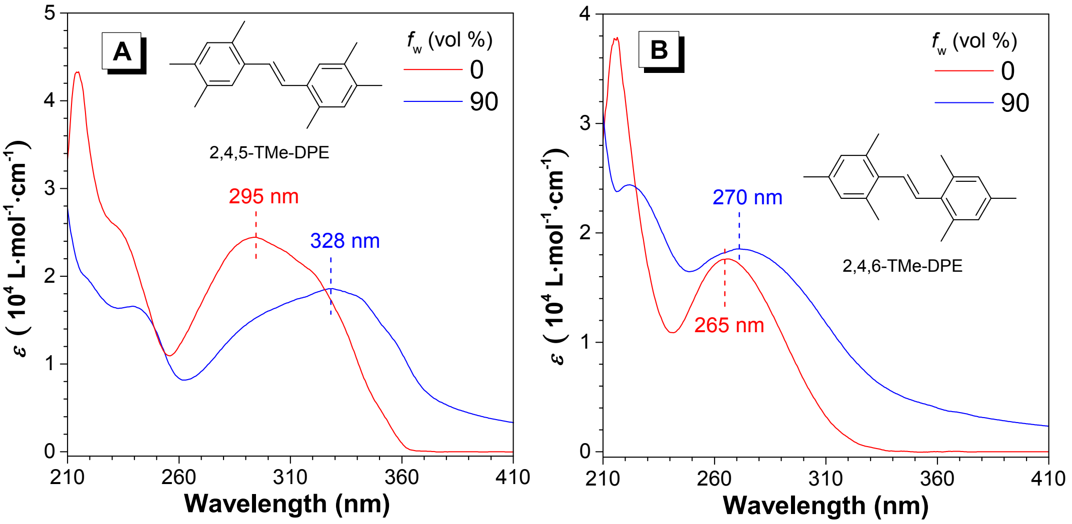

Figure S24. Absorption spectra of (A) 2,4,5-TMe-DPE and (B) 2,4,6-TMe-DPE in THF/water mixtures with water fractions (f_w) = 0 and 90%. Concentration=10^{-4} M.

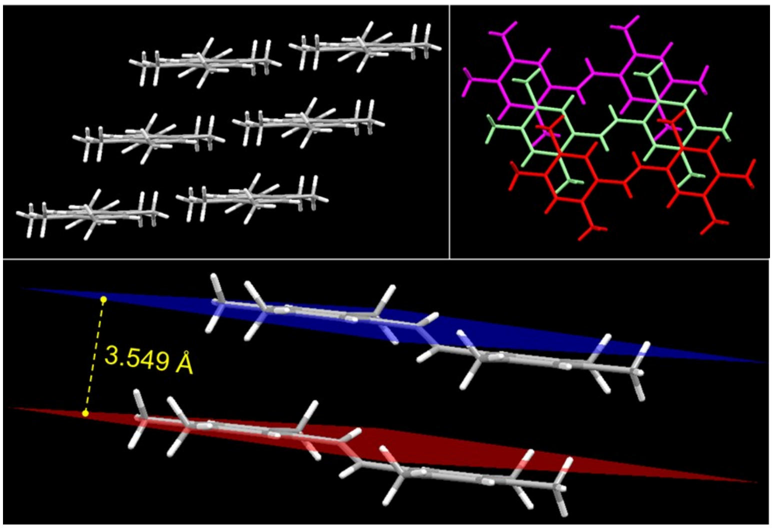

Figure S25. Crystal packing structures of 2,4,5-TMe-DPE.

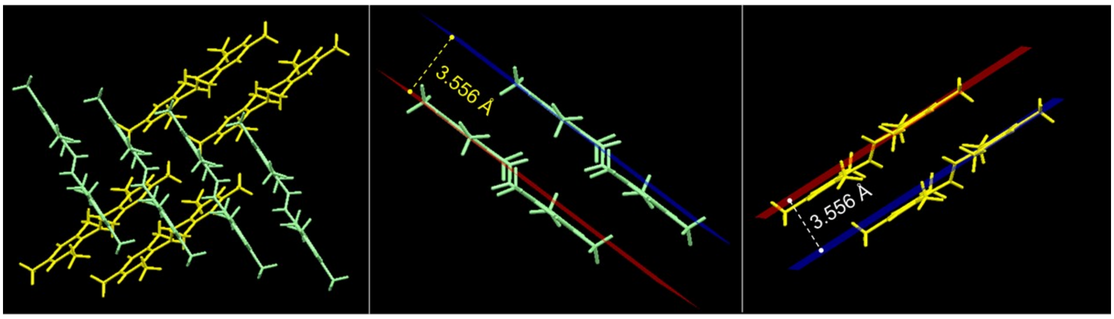

Figure S26. Crystal packing structures of 2,4,6-TMe-DPE.

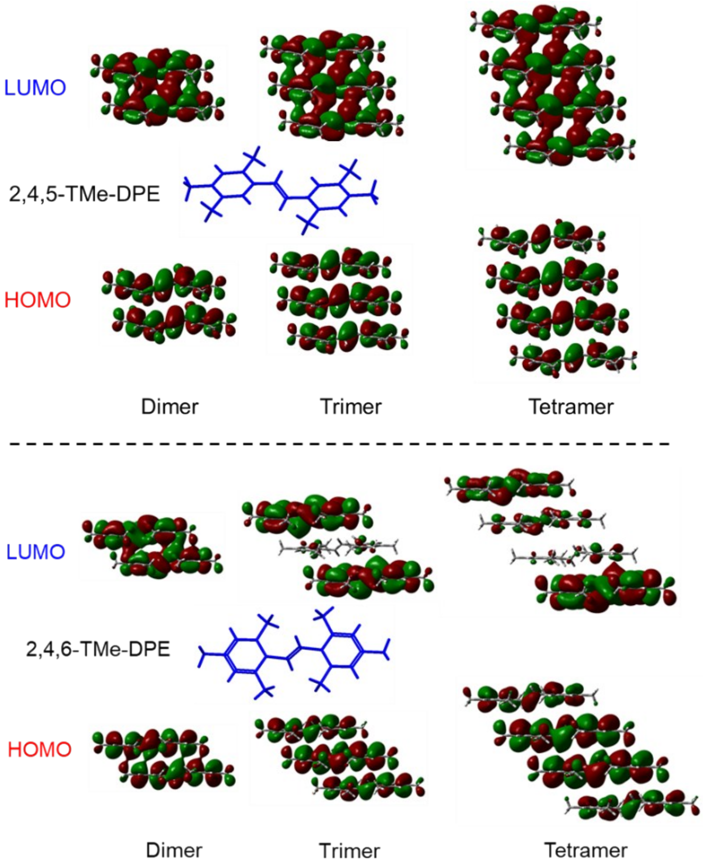

Figure S27. Frontier molecular orbitals of the dimer, trimer and tetramer of 2,4,5-TMe-DPE, 2,4,6-TMe-DPE in the ground state calculated by DFT B3LYP/6-31G**, Gaussian 09 program. Isovalue = 0.01 e/Å^3.

Time-resolved fluorescence spectroscopy

The samples were excited with a femtosecond optical parametric amplifier (Coherent OPerA Solo) pumped by an amplified Ti:sapphire system (Coherent Legend Elite system), at a wavelength of 290 nm. The laser power was adjusted with a variable neutral density filter. A 300-nm long pass filter was used to cut the laser scatter. Time-resolved spectra were captured using a Hamamatsu streak camera (Hamamatsu C4334), the emission intensity from the streak camera was integrated over 30 nm spectrally, centering at the emission peak of the sample, and subsequently plotted with the corresponding time coordinates.

Time-resolved fluorescence spectroscopy is a widely used technique to study the fluorescence of a sample monitored as a function of time after excitation by a pulse of light. This technique uses convolution integral to calculate a lifetime from a fluorescence decay. As shown in Figure S28, the fluorescence decay curve could be fitted with an ExpDecay1 function and the fluorescence decay lifetime (τ) was calculated to be 390 ps for 2,4,5-TMe-DPE whose $\Phi_{F,\ solution}$ is 13.4%. However, the decay curves of 2,4,6-TMe-DPE and laser source were almost completely overlapped, which indicated that the excited-state emission was very weak and ultrafast in twisted 2,4,6-TMe-DPE and the τ was hard to be quantified accurately. In general, time-resolved fluorescence spectroscopy can only detect the photon transition between the excited and ground state, but the signal cannot be observed anymore once the excited state is gone. In comparison, fs-TA can capture the changes of ground and excited state, which makes the evolution of non-emissive states and dark states detectable. In other word, fs-TA is a suitable tool to study the k_{nr} in nonluminescent system with a high temporal resolution.

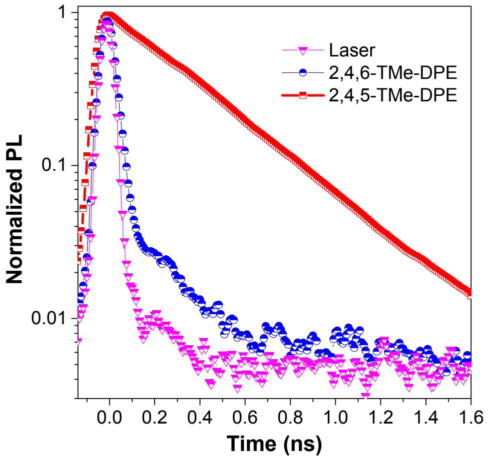

Figure S28. Time-resolved fluorescence decay curves of 2,4,6-TMe-DPE and 2,4,5-TMe-DPE in THF solution with a 290 nm laser source excitation. System limited (~30ps) decay curve of laser source was also recorded for reference. These plots have been smoothed with Adjacent-Averaging method.

Four-point Calculation:

We carried out the geometrical optimization and frequencies calculation for S_0 and S_1 states in the gas phase at (TD)B3LYP/6-311G(d,p) level. The calculation details through the four-point method are shown below.

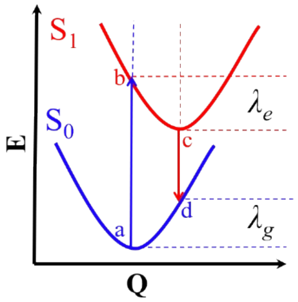

As shown in the schematic potential energy profiles of S_0 and S_1 states, point **a** and **c** stand for $S_{0\mathrm{min}}$ and $S_{1\mathrm{min}}$, respectively. Point **b** and **d** stand for the relevant energy levels from the vertical excitation. The reorganization energy on the potential energy profiles of S_0 and S_1 states are deduced using the following equation:

$$\lambda_e = E(\mathrm{b}) - E(\mathrm{c})$$
$$\lambda_g = E(\mathrm{d}) - E(\mathrm{a})$$

The results from the four-point method for reorganization energy are shown below.

(cm^{-1})	2,4,5-TMe-DPE	2,4,5-TMe-DPE
λ_g	2271	4689
λ_e	3265	5577

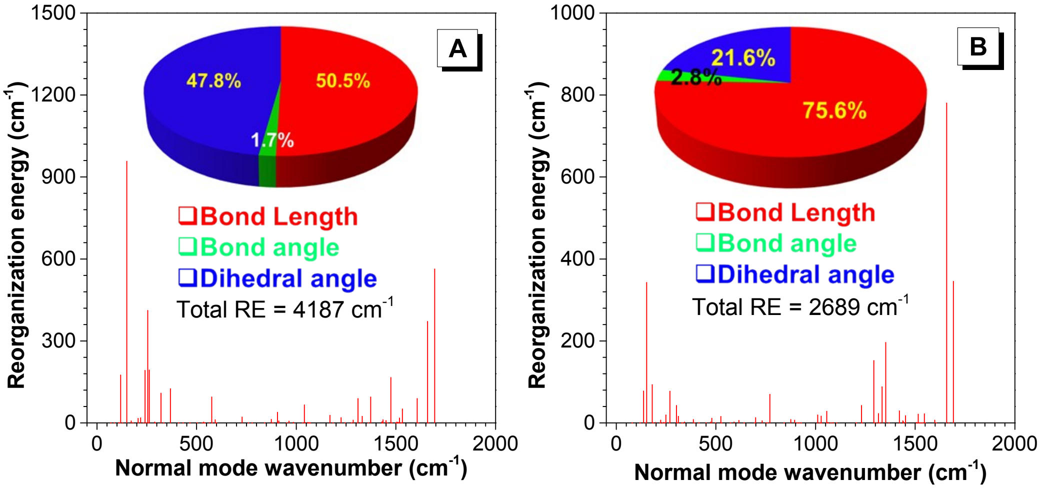

Figure S29. Plot of calculated reorganization energy versus the normal mode wavenumber of (A and B) 2,4,6-TMe-DPE and (B) 2,4,5-TMe-DPE in the crystal state calculated by the TD-DFT, B3LYP/6-311G** and Gaussian 09 program. Inset: contribution of bond length, bond angle and dihedral angle to the total reorganization energy.

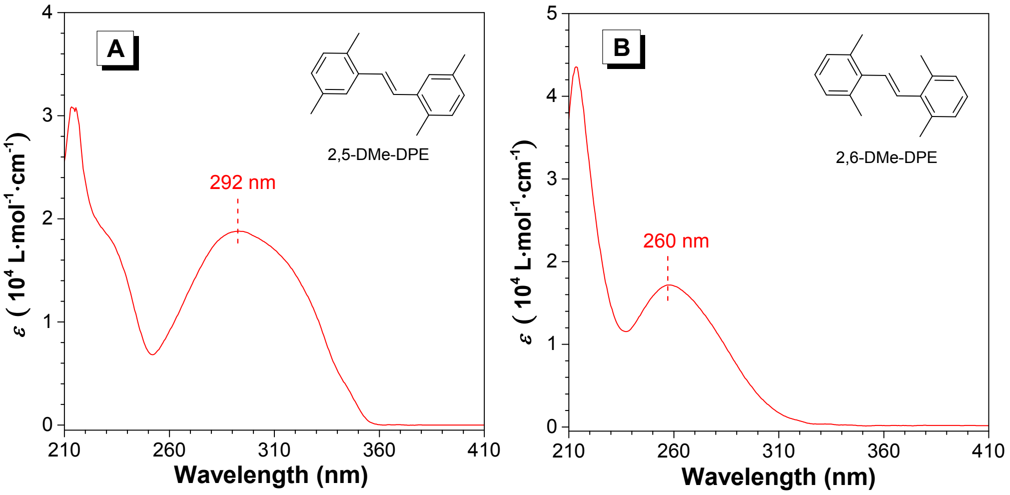

Figure S30. Absorption spectra of (A) 2,5-DMe-DPE and (B) 2,6-DMe-DPE in THF. Concentration =10^{-5} M.

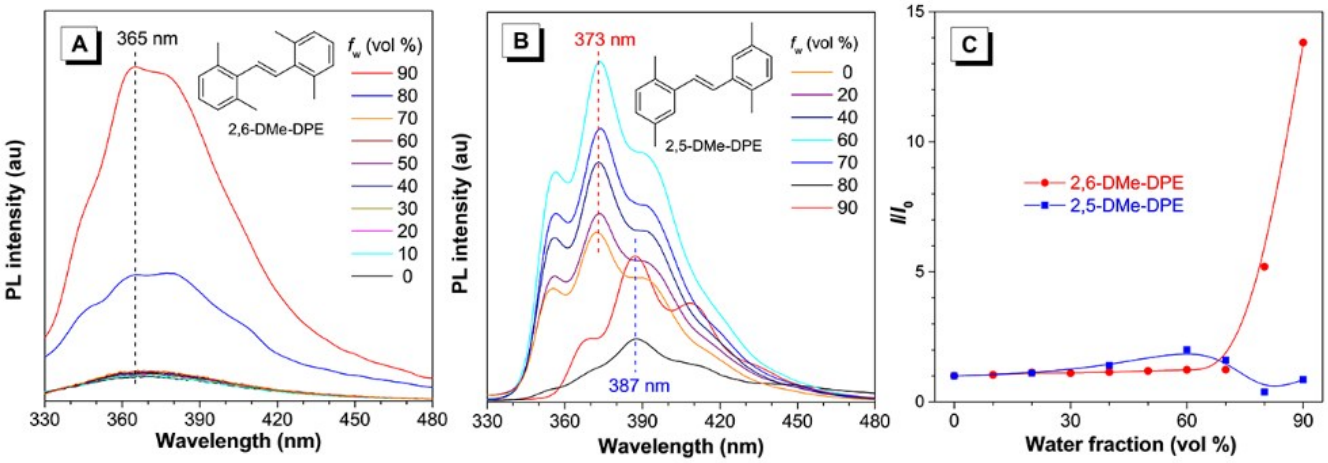

Figure S31. PL spectra of (A) 2,6-DMe-DPE and (B) 2,5-DMe-DPE in THF/water mixtures with different water fractions (f_w). (C) Plots of relative PL intensity (I/I_0) of 2,6-DMe-DPE and 2,5-DMe-DPE versus the composition of their THF/water mixture. Concentration = 10 μM, λ_{ex} = 280 nm, I_0 = PL intensity at f_w = 0%.

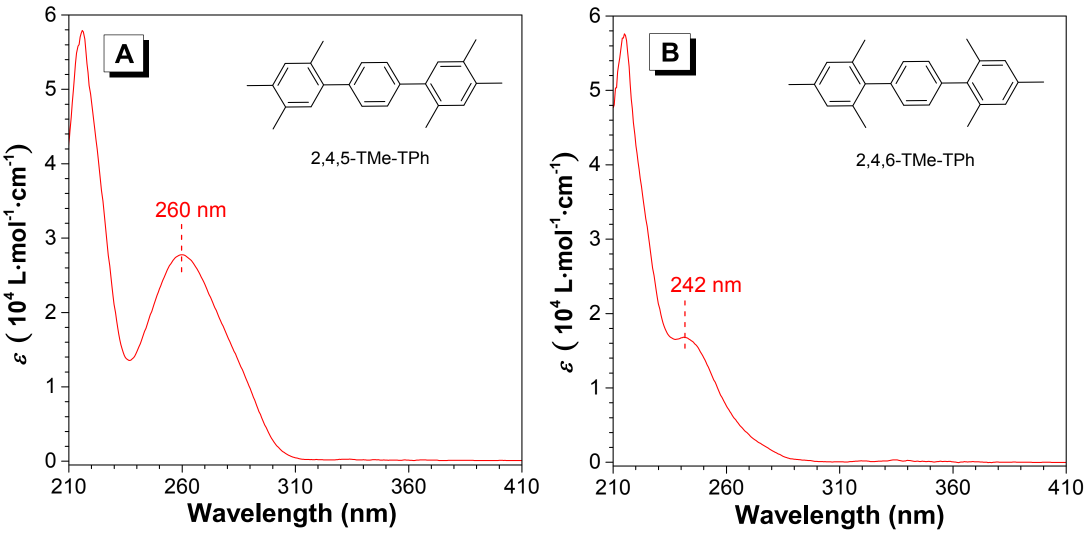

Figure S32. Absorption spectra of (A) 2,4,5-TMe-TPh and (B) 2,4,6-TMe-TPh in THF. Concentration $=10^{-5}$ M.

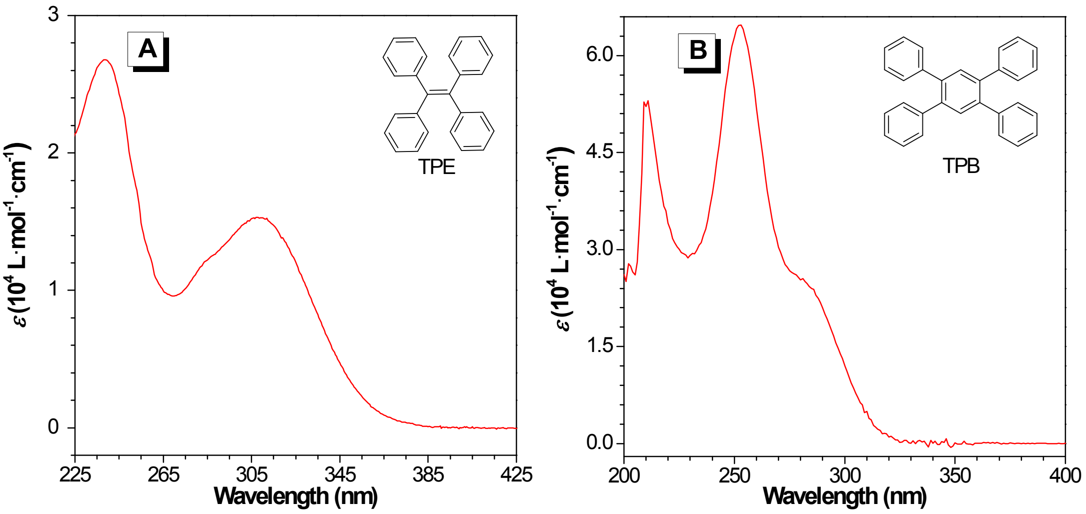

Figure S33. Absorption spectra of (A) TPE and (B) TPB in THF. Concentration $=10^{-5}$ M.